

Fully differential W' production and decay at next-to-leading order in QCD

Zack Sullivan

Theoretical Physics Department, Fermi National Accelerator Laboratory, Batavia, IL, 60510-0500
(July 23, 2002)

We present the fully differential production and decay of a W' boson, with arbitrary vector and axial-vector couplings, to any final state at next-to-leading order in QCD. We demonstrate a complete factorization of couplings at next-to-leading order in both the partial width of the W' boson, and in the full two-to-two cross section. We provide numerical predictions for the contribution of a W' boson to single-top-quark production, and separate results based on whether the mass of the right-handed neutrino ν_R is light enough for the leptonic decay channel to be open. The single-top-quark analysis will allow for an improved direct W' mass limit of 525–550 GeV using data from run I of the Fermilab Tevatron. We propose a modified tolerance method for estimating parton distribution function uncertainties in cross sections.

I. INTRODUCTION

Since the introduction of the standard model, many extensions have been proposed that involve enhanced gauge symmetries. One common feature of these models is the prediction of additional gauge bosons, generically called W' and Z' bosons. In non-universal and top-flavor models, the W' gauge boson arises from a new $SU(2)_L$ sector that distinguishes between generations of fermions [1–3], and may treat quarks and leptons differently [4–6]. The W' boson could be the lowest Kaluza-Klein mode of the W boson [7], or a heavy mass eigenstate in non-commuting extended technicolor [8]. In a left-right symmetric model the W' and standard-model W bosons are remnants of a broken $SU(2)_L \times SU(2)_R$ symmetry [9–12]. The resulting left-right mixing may be naturally suppressed by orbifold breaking of the left-right symmetry [13], or by supersymmetric interactions [14]. While indirect bounds may be placed on the masses and couplings of these various W' bosons within the context of their explicit theories, it is always advantageous to search for these new particles directly. In order to facilitate a direct experimental search, and to achieve the most general contact with theory, we calculate the fully differential next-to-leading order cross section for the production and decay of a W' boson to any final state with arbitrary vector and axial-vector couplings.

The most general Lorentz invariant Lagrangian describing the coupling of a W' to fermions may be written as

$$\mathcal{L} = \frac{g}{\sqrt{2}} \bar{f}_i \gamma_\mu (C_{f_i f_j}^R P_R + C_{f_i f_j}^L P_L) W' f_j + \text{H.c.}, \quad (1)$$

where $P_{R,L} = (1 \pm \gamma_5)/2$, g is the standard model $SU(2)_L$ coupling, and the $C_{f_i f_j}^{R,L}$ are arbitrary couplings that differ for quarks and leptons. For a standard model W boson, $C^R = 0$, and C^L is either the Cabibbo-Kobayashi-Maskawa matrix or diagonal, for quarks or leptons, respectively.

Most experimental searches have concentrated on W' bosons that decay via a purely left- or right-handed current. In order to make contact with these results, we rewrite Eq. (1) in the notation typical of left-right symmetric models as [15]

$$\mathcal{L} = \frac{1}{\sqrt{2}} \bar{f}_i \gamma_\mu (g_R e^{i\omega} \cos \zeta V_{f_i f_j}^R P_R + g_L \sin \zeta V_{f_i f_j}^L P_L) W' f_j + \text{H.c.}, \quad (2)$$

where ζ is a left-right mixing angle, and ω is a CP-violating phase that can be absorbed into V^R . In this notation, $g_{R(L)}$ are the right (left) gauge couplings, and $V_{f_i f_j}^{R,L}$ are generalized Cabibbo-Kobayashi-Maskawa (GCKM) matrices. In models where the W and W' mix, the mixing angle ζ is usually constrained to be small ($|\zeta| < \text{a few } \times 10^{-5} - 10^{-2}$ [16]). Hence, the search for purely right- or left-handed states appears well motivated.

Many direct searches for W' bosons have been performed at hadron colliders. Most experimental analyses have considered left- or right-handed W' bosons, with standard-model-like couplings, that decay into leptonic final states. Left-handed W'_L bosons, or right-handed W'_R bosons in which the decay into a right-handed neutrino ν_R is kinematically allowed, are constrained to have masses $m_{W'} > 786$ GeV [17–24]. If $m_{\nu_R} \gtrsim m_{W'}$ the decay to ν_R is not allowed, and the right-handed W'_R bosons are only directly constrained by peak searches in the dijet data. Unless the W' has greatly enhanced couplings to light quarks, the dijet data are limited by QCD backgrounds to providing a mass limit of 420 GeV [25–27].

The only final state not measured by one of the experiments listed above involves the decay of a W' to a single top quark. In Refs. [28,29] it was pointed out that a deviation of measured the single-top-quark cross section from the

standard model prediction could be evidence of a new gauge interaction. In the context of models with W' bosons, we wish to take this one step further, and propose that the experiments search for an explicit W' mass peak in the s -channel single-top-quark sample. We examine just how large the cross section into single top quarks can be at the Fermilab Tevatron and Large Hadron Collider (LHC) as a function of W' mass, and determine how enhanced or suppressed couplings enter into the measurable cross section after cuts. We also determine the next-to-leading order distributions of the final-state jets to estimate the effect on the reconstruction of the W' mass peak.

A W' boson that propagates in the s -channel appears very similar to Drell-Yan production. We might be tempted to use the next-to-next-to-leading order (NNLO) predictions for Drell-Yan [30] (or the updates in Ref. [31]). However, these calculations are not adequate to predict the cross section for W' bosons which decay to quarks. There are two reasons for this. The first problem is that the final state effects are very large. Not only are there large QCD corrections to the quark final state, but the top-quark mass has a large effect on the branching fraction when it is in the final state. The second reason is that there are initial- and final-state interference terms that arise at NNLO that are of an unknown size. (Pure QCD processes also interfere at NNLO, e.g. with $u\bar{d} \rightarrow u\bar{d}$ via the exchange of two gluons.) Therefore, we cannot simply take the NNLO production as calculated and append a Breit-Wigner propagator that uses leading or next-to-leading order widths. Instead, we perform the complete calculation at next-to-leading order.

We organize the paper as follows. In Sec. II we calculate the partial widths into leptons or quarks, including the effects of the top-quark mass, for the W' boson using arbitrary vector and axial-vector couplings at next-to-leading order (NLO) in QCD. We demonstrate that the couplings factorize, and present some numerical results for partial widths and branching fractions into a top-quark final state. In Sec. III we calculate the fully differential production and decay of a W' into any final state at NLO in QCD. We present numerical results for the single-top-quark production cross section via s -channel exchange of a W' boson. We assess all theoretical uncertainties, and propose a modification of the tolerance method for calculating parton distribution function uncertainties. Finally, we present the NLO jet distributions, discuss the effect of jet definitions on these distributions, and estimate the limits that may be placed on the W' mass using data from run I and run II of the Fermilab Tevatron.

II. NEXT-TO-LEADING ORDER WIDTH

We divide our evaluation of the W' width into three terms that depend on the final decay products:

$$\Gamma_{\text{tot}}(W') = \Gamma(W' \rightarrow t\bar{q}') + \Gamma(W' \rightarrow q\bar{q}') + \Gamma(W' \rightarrow l\bar{\nu}). \quad (3)$$

We separate the partial widths containing a top quark from those containing only massless quarks so that we may retain an explicit top-quark mass dependence in the width.

While the large number of couplings in Eq. (2) appears daunting, a factorization of the couplings occurs in the partial widths of Eq. (3) that greatly simplifies the calculation. The leading order partial widths are

$$\Gamma_{\text{LO}}(W' \rightarrow t\bar{q}') = \frac{g^2\beta^2}{16\pi m_{W'}} |V'_{tq'}|^2 (m_{W'}^2 + m_t^2/2), \quad (4)$$

$$\Gamma_{\text{LO}}(W' \rightarrow q\bar{q}') = \frac{g^2}{16\pi} |V'_{qq'}|^2 m_{W'}, \quad (5)$$

$$\Gamma_{\text{LO}}(W' \rightarrow l\bar{\nu}) = \frac{g^2}{16\pi} |V'_{l\nu}|^2 \frac{m_{W'}}{3}, \quad (6)$$

where $\beta = 1 - m_t^2/m_{W'}^2$, and we assume $g^2 = 8m_W^2 G_F/\sqrt{2}$, as in the standard model. Because we have assumed there is at most one non-zero mass in the final state, the couplings appear only in the combination

$$|gV'_{f_i f_j}|^2 \equiv |g_L \sin \zeta V_{f_i f_j}^L|^2 + |g_R \cos \zeta V_{f_i f_j}^R|^2. \quad (7)$$

Hence, the partial widths of the W' boson have the same form as the standard model W boson, with the effect of new couplings and GCKM matrix elements absorbed into $V'_{f_i f_j}$.

The above factorization of couplings turns out to hold in the next-to-leading order widths as well. The calculations of the next-to-leading order partial widths of the W boson were first performed for the massless [32], one mass [33], and arbitrary mass [34] final states many years ago. In order to derive the factorization of arbitrary couplings above, however, we rederive the partial widths, but use a newer calculational method whose results are needed in the calculation of the fully differential cross section in Sec. III.

We evaluate the next-to-leading order partial widths to quarks by using the phase-space-slicing method with two cutoffs [35]. In this method, phase space is divided into three regions: soft (S), hard collinear (HC), and hard non-collinear (HC \bar{C}). The first two regions are integrated over two-body phase space in $n = 4 - 2\epsilon$ dimensions, whereas the third region is integrated over three-body phase space in 4 dimensions with cuts.

The soft region of phase space is defined in the W' rest frame by a condition on the energy of the emitted gluon

$$E_g \leq \delta_s \frac{m_{W'}}{2}, \quad (8)$$

where δ_s is an arbitrary parameter that must cancel in the final result. The hard region is the complement, $E_g > \delta_s m_{W'}/2$. The gluon can only be collinear with a light quark, and so the collinear region is defined by comparing the invariant mass squared of the gluon and light quark to $\delta_c m_{W'}^2$, i.e. the collinear region is $s_{qg} = 2p_q \cdot p_g < \delta_c m_{W'}^2$, where $p_{q,g}$ are quark and gluon four-momenta. The final result must be independent of δ_c . In practice we retain terms logarithmic in δ_s or δ_c , and drop terms that are linear in the cutoffs. At the end, we take the couplings numerically to zero and show the solution contains no residual δ_s or δ_c dependence.

The two-body next-to-leading order correction to the width is given by

$$\delta\Gamma_2 = \frac{\alpha_s(m_{W'})}{2\pi} C_F (M_S^2 + M_C^2 + M_V^2 + \widetilde{M}_V^2) \Gamma_{\text{LO}}, \quad (9)$$

where $C_F = 4/3$, and Γ_{LO} is listed in Eqs. (4, 5). If there is a top quark in the final state, the terms are

$$M_S^2 = 2 \ln^2(\delta_s) - 2 \ln(\delta_s) \left[1 - \ln\left(\frac{m_{W'}^2}{m_t^2}\right) \right] + \frac{m_{W'}^2 + m_t^2}{m_{W'}^2 - m_t^2} \ln\left(\frac{m_{W'}^2}{m_t^2}\right) - 2\text{Li}_2(\beta) - \frac{1}{2} \ln^2\left(\frac{m_{W'}^2}{m_t^2}\right), \quad (10)$$

$$M_C^2 = \frac{7}{2} - 2\zeta_2 - \ln^2(\delta_s) + 2\text{Li}_2\left(\frac{\beta\delta_c}{\delta_s}\right) - \ln^2(\beta) + 2 \ln(\delta_s) \ln(\beta) - \ln(\delta_c) \left(2 \ln(\delta_s) + \frac{3}{2} - 2 \ln(\beta) \right), \quad (11)$$

$$M_V^2 = -\frac{1}{2} \ln^2\left(\frac{m_{W'}^2}{m_t^2}\right) - \frac{5}{2} \ln\left(\frac{m_{W'}^2}{m_t^2}\right) - \ln(1 - \lambda) \left[2 + \beta + 2 \ln\left(\frac{m_{W'}^2}{m_t^2}\right) \right] - 6 - \ln^2(1 - \lambda) + 2\text{Li}_2(\lambda) - 2\zeta_2, \quad (12)$$

$$\widetilde{M}_V^2 = \frac{\beta(1 - \beta)}{2(3 - \beta)} \ln(1 - \lambda), \quad (13)$$

where $\zeta_2 = \pi^2/6$, $\beta = 1 - m_t^2/m_{W'}^2$, and $\lambda = 1/\beta$. Note $(1 - \lambda) < 0$, which means $\ln(1 - \lambda) = \ln|1 - \lambda|$, but $\ln^2(1 - \lambda) = \ln^2|1 - \lambda| - \pi^2$.

If both final-state quarks are massless, the formulae simplify to

$$M_S^2 = 4 \ln^2(\delta_s), \quad (14)$$

$$M_C^2 = 7 - 4\zeta_2 - 2 \ln^2(\delta_s) + 4\text{Li}_2\left(\frac{\delta_c}{\delta_s}\right) - \ln(\delta_c)[4 \ln(\delta_s) + 3], \quad (15)$$

$$M_V^2 = -8 + 4\zeta_2, \quad (16)$$

$$\widetilde{M}_V^2 = 0. \quad (17)$$

The sum of the terms in the massless case is

$$M^2 = 2 \ln^2(\delta_s) - \ln(\delta_c)[4 \ln(\delta_s) + 3] + 4\text{Li}_2\left(\frac{\delta_c}{\delta_s}\right) - 1. \quad (18)$$

The three-body hard non-collinear real gluon emission term is evaluated using a Monte Carlo integration in four dimensions, subject to the cuts listed above. The integrand is given by

$$d(\delta\Gamma_3) = \frac{1}{64\pi^3 m_{W'}} \overline{\Sigma} |M_3|^2 dE_g dE_{q'}, \quad (19)$$

with

$$\overline{\Sigma} |M_3|^2 = -2\pi\alpha_s g^2 C_F |V'_{tq'}|^2 \Psi_\Gamma, \quad (20)$$

and

$$\begin{aligned} \Psi_\Gamma = & 2\beta m_{W'}^2 (3 - \beta) \left(\frac{s'_{12}}{s_{13}s'_{23}} - \frac{m_t^2}{s'_{23}} \right) \\ & + (3 - \beta) \left(\frac{s_{13}}{s'_{23}} + \frac{s'_{23}}{s_{13}} \right) + 2(1 - \beta), \end{aligned} \quad (21)$$

where $\beta = 1 - m_t^2/m_{W'}^2$, $s'_{12} = 2p_1 \cdot p_2$, $s_{13} = 2p_1 \cdot p_3$, $s'_{23} = 2p_2 \cdot p_3$, and p_1 , p_2 , and p_3 are the four-momenta of the light quark, top quark, and gluon, respectively. When both quarks are massless $\beta = 1$, and Eq. (21) is very simple.

Once we determine that the factorization of couplings holds for all terms, the partial widths reduce to the expressions given in Ref. [33] with the replacement of CKM matrix elements by the GCKM matrix elements $|V'|^2$ defined in Eq. (7). The massless case is simply

$$\Gamma_{\text{NLO}}(W' \rightarrow q\bar{q}') = \left(1 + \frac{\alpha_s(m_{W'})}{\pi} \right) \Gamma_{\text{LO}}(W' \rightarrow q\bar{q}'). \quad (22)$$

The massive case should reduce to Eq. (12) of Ref. [33],

$$\begin{aligned} \Gamma_{\text{NLO}}(W' \rightarrow t\bar{q}') = & \Gamma_{\text{LO}}(W' \rightarrow t\bar{q}') + \frac{g^2}{16\pi} \frac{\alpha_s(m_{W'})}{4\pi} C_F |V'_{tq'}|^2 m_{W'} \\ & \times \{ \beta(1 - \beta)(\beta - 4) - \beta^2(9 - 5\beta) \ln(\beta) - (1 - \beta)(4 + 6\beta - 5\beta^2) \ln(1 - \beta) \\ & + \beta^2(3 - \beta)[3/2 + 4\text{Li}_2(1 - \beta) + 2 \ln(\beta) \ln(1 - \beta)] \}. \end{aligned} \quad (23)$$

A. Numerical results

In order to be of immediate use to experimental analyses at the Fermilab Tevatron, we make definite predictions of the W' partial and total widths. In all numerical results we use $m_t = 175 \pm 5$ GeV, $G_F = 1.16639 \times 10^{-5}$ GeV⁻², and $m_W = 80.4$ GeV. We use a two-loop running of α_s as defined in the CTEQ5M1 parton distribution functions [36]. We assume that $V'_{\nu\nu}$ is the identity matrix, and for $V'_{qq'}$ we use the average Cabibbo-Kobayashi-Maskawa (CKM) matrix [16] with the exception that we assume $|V'_{tb}| = 1$,

$$V'_{\text{CKM}} = \begin{pmatrix} 0.9751 & 0.2215 & 0.0035 \\ 0.2210 & 0.9743 & 0.0410 \\ 0.0090 & 0.0400 & 1.0000 \end{pmatrix}. \quad (24)$$

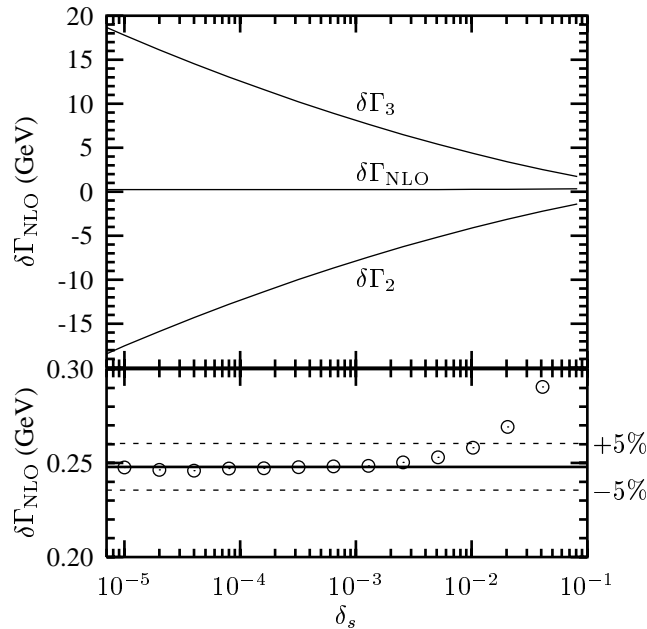


FIG. 1. Dependence of the NLO correction to the W' width on $\delta_s = 300 \times \delta_c$, for $m_{W'} = 500$ GeV. $\delta\Gamma_{\text{NLO}} = \delta\Gamma_2 + \delta\Gamma_3$, where $\delta\Gamma_3$ refers to the $\text{H}\bar{\text{C}}$ component, and $\delta\Gamma_2$ to the sum of virtual, soft and hard-collinear contributions. The bottom region shows an enlargement of the numerical prediction (circles) compared to the analytic prediction (solid line) in Eq. (23).

Before we discuss our results, we must show that our final result does not depend on the cutoffs we choose. To demonstrate this, we fix the ratio of $\delta_s/\delta_c = 300$, and plot in Fig. 1 the NLO correction to the width of a W' of mass 500 GeV. In the upper half of the figure we see the logarithmic dependence in δ_s and δ_c of the two- and three-body terms, $\delta\Gamma_2$ and $\delta\Gamma_3$. In the bottom half of the figure we focus on the sum of the correction terms $\delta\Gamma_{\text{NLO}}$ for various values of δ_s (circles), and compare the result to the analytic prediction (solid line) of Eq. (23). Once $\delta_s \lesssim 10^{-3}$ ($\delta_c \lesssim 1/3 \times 10^{-5}$), the result is stable to much less than 1% of the known NLO correction. In practice there is a tradeoff between numerical accuracy in canceling the logarithmic divergences of δ_s and δ_c in the Monte Carlo, and the residual power suppressed dependence on these parameters. Hence, we always choose values of δ_s and δ_c to ensure that the residual effects are smaller than the desired Monte Carlo statistical error.

In Table I we list the LO and NLO partial widths for the decay of the W' into light quarks, or $t\bar{b}$. Since we assume the standard model-like couplings of Eq. (24), the decays into $t\bar{d}$ and $t\bar{s}$ are strongly suppressed. However, we remind the reader that any model may be restored via the use of Eq. (7). We present the results for W' masses between 200 GeV and 1000 GeV, in order to cover the possible reach of experiments at the Tevatron.

TABLE I. LO and NLO partial widths for W' decays into light quarks, or $t\bar{b}$.

Mass (GeV)	$\Gamma_{\text{LO}}(W' \rightarrow q\bar{q}') \text{ (GeV)}$	$\Gamma_{\text{NLO}}(W' \rightarrow q\bar{q}') \text{ (GeV)}$	$\Gamma_{\text{LO}}(W' \rightarrow t\bar{b}) \text{ (GeV)}$	$\Gamma_{\text{NLO}}(W' \rightarrow t\bar{b}) \text{ (GeV)}$
200	1.697	1.754	0.129	0.166
225	1.909	1.973	0.388	0.473
250	2.121	2.191	0.687	0.811
275	2.333	2.409	0.993	1.146
300	2.546	2.628	1.296	1.471
350	2.970	3.064	1.879	2.084
400	3.394	3.500	2.432	2.655
450	3.818	3.936	2.959	3.196
500	4.243	4.372	3.467	3.715
550	4.667	4.807	3.961	4.218
600	5.091	5.243	4.443	4.710
650	5.515	5.678	4.917	5.192
700	5.940	6.114	5.384	5.667
750	6.364	6.549	5.845	6.136
800	6.788	6.984	6.301	6.600
850	7.212	7.420	6.754	7.061
900	7.637	7.855	7.204	7.518
950	8.061	8.290	7.651	7.972
1000	8.485	8.725	8.096	8.425

Unless the couplings are suppressed, a left-handed W' will decay into either quarks or leptons. A right-handed W' , however, will decay to leptons only if the mass of the right-handed neutrino (m_{ν_R}) is less than $m_{W'}$, or if there is large left-right mixing in the neutrino sector. For completeness, we consider both kinematic cases. In Tables II and III we list the LO and NLO W' total widths and branching fractions into a $t\bar{b}$ final state. We assume a top-quark mass of 175 GeV. The largest uncertainty in the predictions of both the total width and the branching fractions is a result of the uncertainty in the top-quark mass. Hence, we also show the increase (upper error), or decrease (lower error), in the quantities if the top-quark mass is 170 GeV, or 180 GeV, respectively. In Table II we include only the decays into quark final states. In Table III we allow for the decay into quarks or leptons as in the standard model. The total widths in these Tables are used in Sec. III in the NLO calculation of the W' contribution to the single-top-quark cross section.

TABLE II. Total width of the W' , and its branching ratio into $t\bar{b}$, at LO and NLO in QCD, when the decay to leptons is not allowed. Errors are due to the top-quark mass uncertainty, $m_t = 175 \mp 5$ GeV.

Mass (GeV)	Γ_{LO} (GeV)	$\text{BR}_{\text{LO}}(W' \rightarrow t\bar{b})$	Γ_{NLO} (GeV)	$\text{BR}_{\text{NLO}}(W' \rightarrow t\bar{b})$
200	3.523 $^{+0.049}_{-0.043}$	0.0366 $^{+0.0132}_{-0.0119}$	3.675 $^{+0.060}_{-0.053}$	0.0452 $^{+0.0152}_{-0.0140}$
225	4.206 $^{+0.064}_{-0.061}$	0.0923 $^{+0.0136}_{-0.0135}$	4.419 $^{+0.073}_{-0.071}$	0.1071 $^{+0.0144}_{-0.0146}$
250	4.930 $^{+0.068}_{-0.067}$	0.1394 $^{+0.0117}_{-0.0119}$	5.193 $^{+0.074}_{-0.074}$	0.1561 $^{+0.0119}_{-0.0122}$
275	5.660 $^{+0.067}_{-0.068}$	0.1755 $^{+0.0097}_{-0.0100}$	5.965 $^{+0.071}_{-0.072}$	0.1922 $^{+0.0095}_{-0.0099}$
300	6.388 $^{+0.065}_{-0.066}$	0.2030 $^{+0.0081}_{-0.0083}$	6.726 $^{+0.067}_{-0.068}$	0.2187 $^{+0.0077}_{-0.0080}$
350	7.819 $^{+0.059}_{-0.060}$	0.2404 $^{+0.0057}_{-0.0059}$	8.211 $^{+0.058}_{-0.060}$	0.2537 $^{+0.0053}_{-0.0055}$
400	9.220 $^{+0.053}_{-0.054}$	0.2637 $^{+0.0042}_{-0.0044}$	9.654 $^{+0.051}_{-0.052}$	0.2750 $^{+0.0038}_{-0.0040}$
450	10.595 $^{+0.048}_{-0.049}$	0.2792 $^{+0.0032}_{-0.0033}$	11.068 $^{+0.045}_{-0.046}$	0.2888 $^{+0.0029}_{-0.0030}$
500	11.952 $^{+0.043}_{-0.044}$	0.2901 $^{+0.0026}_{-0.0027}$	12.458 $^{+0.040}_{-0.041}$	0.2982 $^{+0.0022}_{-0.0023}$
550	13.294 $^{+0.040}_{-0.041}$	0.2979 $^{+0.0021}_{-0.0022}$	13.832 $^{+0.036}_{-0.037}$	0.3049 $^{+0.0018}_{-0.0019}$
600	14.625 $^{+0.036}_{-0.037}$	0.3038 $^{+0.0017}_{-0.0018}$	15.195 $^{+0.032}_{-0.034}$	0.3099 $^{+0.0015}_{-0.0015}$
650	15.947 $^{+0.034}_{-0.035}$	0.3083 $^{+0.0015}_{-0.0015}$	16.548 $^{+0.030}_{-0.031}$	0.3137 $^{+0.0012}_{-0.0013}$
700	17.263 $^{+0.031}_{-0.032}$	0.3119 $^{+0.0012}_{-0.0013}$	17.894 $^{+0.027}_{-0.028}$	0.3167 $^{+0.0010}_{-0.0011}$
750	18.572 $^{+0.029}_{-0.030}$	0.3147 $^{+0.0011}_{-0.0011}$	19.234 $^{+0.025}_{-0.026}$	0.3190 $^{+0.0009}_{-0.0009}$
800	19.878 $^{+0.027}_{-0.028}$	0.3170 $^{+0.0009}_{-0.0010}$	20.569 $^{+0.023}_{-0.024}$	0.3209 $^{+0.0008}_{-0.0008}$
850	21.179 $^{+0.026}_{-0.026}$	0.3189 $^{+0.0008}_{-0.0009}$	21.900 $^{+0.021}_{-0.023}$	0.3224 $^{+0.0007}_{-0.0007}$
900	22.477 $^{+0.024}_{-0.025}$	0.3205 $^{+0.0007}_{-0.0008}$	23.227 $^{+0.021}_{-0.021}$	0.3237 $^{+0.0006}_{-0.0006}$
950	23.773 $^{+0.023}_{-0.024}$	0.3218 $^{+0.0007}_{-0.0007}$	24.552 $^{+0.020}_{-0.019}$	0.3247 $^{+0.0005}_{-0.0005}$
1000	25.066 $^{+0.022}_{-0.023}$	0.3230 $^{+0.0006}_{-0.0006}$	25.875 $^{+0.018}_{-0.018}$	0.3256 $^{+0.0005}_{-0.0005}$

TABLE III. Total width of the W' , and its branching ratio into $t\bar{b}$, at LO and NLO in QCD, when decays to quarks or leptons are both included. Errors are due to the top-quark mass uncertainty, $m_t = 175 \mp 5$ GeV.

Mass (GeV)	Γ_{LO} (GeV)	$\text{BR}_{\text{LO}}(W' \rightarrow t\bar{b})$	Γ_{NLO} (GeV)	$\text{BR}_{\text{NLO}}(W' \rightarrow t\bar{b})$
200	5.220 $^{+0.049}_{-0.043}$	0.0247 $^{+0.0091}_{-0.0081}$	5.372 $^{+0.060}_{-0.053}$	0.0309 $^{+0.0106}_{-0.0097}$
225	6.116 $^{+0.064}_{-0.061}$	0.0635 $^{+0.0097}_{-0.0095}$	6.328 $^{+0.073}_{-0.071}$	0.0748 $^{+0.0105}_{-0.0105}$
250	7.051 $^{+0.068}_{-0.067}$	0.0974 $^{+0.0086}_{-0.0087}$	7.314 $^{+0.074}_{-0.074}$	0.1109 $^{+0.0089}_{-0.0091}$
275	7.994 $^{+0.067}_{-0.068}$	0.1243 $^{+0.0073}_{-0.0075}$	8.298 $^{+0.071}_{-0.072}$	0.1381 $^{+0.0073}_{-0.0076}$
300	8.933 $^{+0.065}_{-0.066}$	0.1451 $^{+0.0062}_{-0.0064}$	9.272 $^{+0.067}_{-0.068}$	0.1587 $^{+0.0060}_{-0.0063}$
350	10.789 $^{+0.059}_{-0.060}$	0.1742 $^{+0.0045}_{-0.0046}$	11.181 $^{+0.058}_{-0.060}$	0.1863 $^{+0.0042}_{-0.0044}$
400	12.614 $^{+0.053}_{-0.054}$	0.1928 $^{+0.0034}_{-0.0035}$	13.049 $^{+0.051}_{-0.052}$	0.2035 $^{+0.0031}_{-0.0032}$
450	14.414 $^{+0.048}_{-0.049}$	0.2053 $^{+0.0026}_{-0.0027}$	14.886 $^{+0.045}_{-0.046}$	0.2147 $^{+0.0023}_{-0.0024}$
500	16.195 $^{+0.043}_{-0.044}$	0.2141 $^{+0.0021}_{-0.0022}$	16.701 $^{+0.040}_{-0.041}$	0.2224 $^{+0.0019}_{-0.0019}$
550	17.961 $^{+0.040}_{-0.041}$	0.2205 $^{+0.0017}_{-0.0018}$	18.499 $^{+0.036}_{-0.037}$	0.2280 $^{+0.0015}_{-0.0015}$
600	19.716 $^{+0.036}_{-0.037}$	0.2253 $^{+0.0014}_{-0.0015}$	20.287 $^{+0.032}_{-0.034}$	0.2322 $^{+0.0012}_{-0.0013}$
650	21.463 $^{+0.034}_{-0.035}$	0.2291 $^{+0.0012}_{-0.0012}$	22.064 $^{+0.030}_{-0.031}$	0.2353 $^{+0.0010}_{-0.0011}$
700	23.202 $^{+0.031}_{-0.032}$	0.2320 $^{+0.0010}_{-0.0011}$	23.834 $^{+0.027}_{-0.028}$	0.2378 $^{+0.0009}_{-0.0009}$
750	24.936 $^{+0.029}_{-0.030}$	0.2344 $^{+0.0009}_{-0.0009}$	25.598 $^{+0.025}_{-0.026}$	0.2397 $^{+0.0007}_{-0.0008}$
800	26.666 $^{+0.027}_{-0.028}$	0.2363 $^{+0.0008}_{-0.0008}$	27.357 $^{+0.023}_{-0.024}$	0.2413 $^{+0.0006}_{-0.0007}$
850	28.391 $^{+0.026}_{-0.026}$	0.2379 $^{+0.0007}_{-0.0007}$	29.113 $^{+0.021}_{-0.023}$	0.2425 $^{+0.0006}_{-0.0006}$
900	30.114 $^{+0.024}_{-0.025}$	0.2392 $^{+0.0006}_{-0.0006}$	30.864 $^{+0.021}_{-0.021}$	0.2436 $^{+0.0005}_{-0.0005}$
950	31.834 $^{+0.023}_{-0.024}$	0.2403 $^{+0.0006}_{-0.0006}$	32.613 $^{+0.020}_{-0.019}$	0.2444 $^{+0.0005}_{-0.0004}$
1000	33.551 $^{+0.022}_{-0.023}$	0.2413 $^{+0.0005}_{-0.0005}$	34.360 $^{+0.018}_{-0.018}$	0.2452 $^{+0.0004}_{-0.0004}$

It is not surprising that top-quark threshold effects cause a large uncertainty in the branching fraction for W' masses less than 300 GeV. This also appears in the large increase in branching fraction at NLO over the LO branching fraction. With 33% changes in both the mass variation and NLO correction, perturbation theory is somewhat suspect if $m_{W'} \sim 200$ GeV. However, the effect is less than 10% by 225 GeV, and rapidly vanishes as $m_{W'}^2 \gg m_t^2$. The branching fraction into a top-quark final state is nearly saturated at 1/3 (1/4) when $m_{W'} \sim 500$ GeV for the quark-only (quark-plus-lepton) model of decays. Hence, a large fraction of W' events should produce a top-quark in the final state. In Sec. III A we see this effect on the single-top-quark cross section.

III. NEXT-TO-LEADING ORDER CROSS SECTION

The analytic form of the differential production and decay of a W' at next-to-leading order is very similar to that of s -channel single-top-quark production. The complete calculation of differential single-top-quark production using the phase space slicing method appears in Ref. [37]. We generalize the calculation in that paper to the production of one massive particle through a W' boson (such that single-top-quark production is a special case). We follow closely the notation of Ref. [37], but retain arbitrary couplings in the vertices. We note that the t -channel exchange of a virtual W' is suppressed by at least $1/m_{W'}^4$, and hence do not consider it here. However, the analytic expressions and factorizations that follow are valid for this channel as well. The analytic formulae for the t -channel exchange may be obtained by simple crossing.

At leading order, the production of a heavy quark (lepton) may be written schematically as

$$u(p_1)\bar{d}(p_2) \rightarrow W'^+ \rightarrow \bar{b}(p_3)t(p_4)[\bar{l}(p_3)\nu(p_4)], \quad (25)$$

where $p_1 + p_2 = p_3 + p_4$, $u\bar{d}$ represents all possible parton fluxes, and the heavy particle in the final state (t or ν_R) has four-momentum p_4 and mass m .

The leading-order fully differential spin-averaged partonic cross section can be written as

$$d\sigma_0 = \frac{1}{2s} \overline{\sum} |\mathcal{M}_0|^2 d\text{PS}_2, \quad (26)$$

where $s = (p_1 + p_2)^2$ is the partonic center-of-momentum energy squared, and the two body phase space is given by

$$d\text{PS}_2 = \frac{1}{(2\pi)^2} \frac{d^3p_3}{2E_3} \frac{d^3p_4}{2E_4} \delta^{(4)}(q - p_3 - p_4). \quad (27)$$

The matrix element squared, summed (averaged) over final- (initial-) state spin and color states, for production of one massive particle is

$$\overline{\sum} |\mathcal{M}_0|^2 = \frac{2N_c}{3} \frac{R_t t(t - m^2) + R_u u(u - m^2)}{(s - m_{W'}^2)^2 + m_{W'}^2 \Gamma_{W'}^2}, \quad (28)$$

where $t = (p_1 - p_3)^2$, $u = (p_2 - p_3)^2$. The number of colors $N_c = 3$, and $m = m_t$, for a final state with a top quark. For the production of a massive neutrino $m = m_{\nu_R}$ and $N_c = 1$. If the final state is massless, simply set $m = 0$ and use $N_c = 3$ (1) for quarks (leptons). The functions R_t and R_u are given by

$$R_t = (|V_i|^2 + |A_i|^2)(|V_f|^2 + |A_f|^2) + 4\text{Re}(V_i A_i^*)\text{Re}(V_f A_f^*), \quad (29)$$

$$R_u = (|V_i|^2 + |A_i|^2)(|V_f|^2 + |A_f|^2) - 4\text{Re}(V_i A_i^*)\text{Re}(V_f A_f^*), \quad (30)$$

where $V_{i,f}$ and $A_{i,f}$ are the vector and axial-vector couplings for the initial- and final-state vertices, respectively. In the notation of Eq. (2),

$$|V|^2 + |A|^2 = \frac{|g_R \cos \zeta V_{f_i f_j}^R|^2 + |g_L \sin \zeta V_{f_i f_j}^L|^2}{4}, \quad (31)$$

$$2\text{Re}(VA^*) = \frac{|g_R \cos \zeta V_{f_i f_j}^R|^2 - |g_L \sin \zeta V_{f_i f_j}^L|^2}{4}. \quad (32)$$

For right- or left-handed W' bosons $|V| = |A|$, $R_u = 0$, R_t reduces to $R_t = (g^4 |V_i|^2 |V_f|^2)/8$, and we recover the standard model s -channel single-top-quark cross section published in Refs. [37,38], including the Breit-Wigner term, up to the GCKM couplings.

We calculate the fully differential next-to-leading order cross section with the same method used in Sec. II. Again, the phase space is divided into a hard and soft region, where the soft region is now defined in the partonic center-of-momentum frame by a condition of the emitted gluon energy:

$$E_g \leq \delta_s \frac{\sqrt{s_{12}}}{2}, \quad (33)$$

where $s_{ij} = (p_i + p_j)^2$. The hard region is the complement, $E_g > \delta_s \sqrt{s_{12}}/2$. A region is collinear if an invariant in a propagator is less than $\delta_c s_{12}$, i.e. the region is collinear if in a denominator we obtain $s_{ij} = (p_i + p_j)^2 < \delta_c s_{12}$, or $t_{ij} = (p_i - p_j)^2 < \delta_c s_{12}$.

At next-to-leading order, color conservation forbids the exchange of a single gluon between the initial and final states. This is convenient when organizing the solution, because the leptonic cross section only has QCD corrections in the initial state. Hence, we list separately the initial and final state corrections.

The two-body NLO correction to the partonic cross section contains

$$d\sigma_2 = \frac{\alpha_s}{2\pi} C_F [(M_S^2 + M_C^2 + M_V^2) d\sigma_0 + d\tilde{\sigma}_V], \quad (34)$$

where $C_F = 4/3$, and $d\tilde{\sigma}_V$ is the part of the correction to the vertex containing the top quark that is not proportional to the LO cross section. If the final state does not contain a top quark then $d\tilde{\sigma}_V = 0$; otherwise,

$$d\tilde{\sigma}_V = (R_t + R_u) \frac{tu}{s^2} \frac{m_t^2 \ln(1-\lambda)}{(s - m_{W'}^2)^2 + m_{W'}^2 \Gamma_{W'}^2} d\text{PS}_2. \quad (35)$$

The initial-state corrections appearing in Eq. (34) are

$$M_{S_i}^2 = 4 \ln^2(\delta_s), \quad (36)$$

$$M_{C_i}^2 = [4 \ln(\delta_s) + 3] \ln\left(\frac{s}{\mu_F^2}\right), \quad (37)$$

$$M_{V_i}^2 = -8 + 4\zeta_2, \quad (38)$$

where $\zeta_2 = \pi^2/6$, and μ_F is the factorization scale. If there is a top quark in the final state, $M_{S_f}^2$, $M_{C_f}^2$, and $M_{V_f}^2$ are the same as those listed in Eqs. (10–12), with the replacements $m_{W'}^2 \rightarrow s$, $\beta \rightarrow 1 - m_t^2/s$, and $\lambda = 1/\beta$. If both quarks in the final state are massless, then M_f^2 is given by Eq. (18).

The complete two-body cross section is given by

$$\sigma_2 = \sum_{a,b} \int dx_1 dx_2 \{ f_a^{H_1}(x_1, \mu_F) f_b^{H_2}(x_2, \mu_F) d\sigma_2^{ab} + [\tilde{f}_a^{H_1}(x_1, \mu_F) f_b^{H_2}(x_2, \mu_F) + f_a^{H_1}(x_1, \mu_F) \tilde{f}_b^{H_2}(x_2, \mu_F)] d\sigma_0^{ab} \}, \quad (39)$$

where a, b sum over all quark-antiquark luminosities, μ_F is the factorization scale, $H_{1,2}$ are the initial-state hadrons, and the $f(x, \mu)$ are NLO parton distribution functions. The \tilde{f} functions are introduced to compensate for a difference between the limits of integration used in the phase space slicing calculation of the initial-state collinear singularities and the modified minimal subtraction $\overline{\text{MS}}$ scheme used in the NLO parton distribution functions. The \tilde{f} functions are given in Ref. [35].

The three-body hard non-collinear terms are evaluated using a Monte Carlo integration in four dimensions, subject to the cuts listed above. The cross section is given by

$$\begin{aligned} \sigma_3 = - \sum_{a,b} \int dx_1 dx_2 \frac{4\pi\alpha_s}{s} \int_{\text{HC}} \{ & f_{q_a}^{H_1}(x_1, \mu_F) f_{q_b}^{H_2}(x_2, \mu_F) \Psi_{q\bar{q}} \\ & + [f_{q_a}^{H_1}(x_1, \mu_F) f_g^{H_2}(x_2, \mu_F) + f_g^{H_1}(x_1, \mu_F) f_{q_b}^{H_2}(x_2, \mu_F)] \Psi_{qg} \} d\text{PS}_3. \end{aligned} \quad (40)$$

If we label the momenta in the three-body processes

$$\Psi_{q\bar{q}} : u(p_1) \bar{d}(p_2) \rightarrow \bar{b}(p_3) t(p_4) g(p_5), \quad (41)$$

$$\Psi_{qg} : u(p_1) g(p_2) \rightarrow \bar{b}(p_3) t(p_4) d(p_5), \quad (42)$$

then functions $\Psi_{q\bar{q}}$ and Ψ_{qg} are given by

$$\Psi_{q\bar{q}} = \frac{2C_F}{(s_{34} - m_{W'}^2)^2 + m_{W'}^2 \Gamma_{W'}^2} \left[R_t \left(-\frac{t'_{24}(t_{13} + s_{35}) - t_{13}t'_{14}}{t_{15}} - \frac{t_{13}(t'_{24} + s'_{45}) - t_{23}t'_{24}}{t_{25}} \right. \right. \\ \left. \left. - \frac{s_{12}[t_{13}(2t'_{24} + s'_{45}) + s_{35}t'_{24}]}{t_{15}t_{25}} \right) + R_u(p_1 \rightleftharpoons p_2) \right] \\ + \frac{2C_F}{(s_{12} - m_{W'}^2)^2 + m_{W'}^2 \Gamma_{W'}^2} \left[R_t \left(-\frac{t'_{24}(t_{13} + t_{15}) - t_{13}t_{23}}{s_{35}} - \frac{t_{13}(t'_{24} + t_{25})(1 - 2m_t^2/s'_{45}) - t'_{14}t'_{24}}{s'_{45}} \right. \right. \\ \left. \left. - \frac{s'_{34}[t_{13}(2t'_{24} + t_{25}) + t_{15}t'_{24}]}{s_{35}s'_{45}} \right) + R_u(p_1 \rightleftharpoons p_2) \right], \quad (43)$$

$$\Psi_{qg} = \frac{1}{(s_{34} - m_{W'}^2)^2 + m_{W'}^2 \Gamma_{W'}^2} \left[R_t \left(\frac{s'_{45}(t_{13} + t_{23}) - t_{13}t'_{14}}{s_{12}} + \frac{t_{13}(s'_{45} + t'_{24}) - s_{35}s'_{45}}{t_{25}} \right. \right. \\ \left. \left. + \frac{t_{15}[s'_{45}(2t_{13} + t_{23}) + t_{13}t'_{24}]}{s_{12}t_{25}} \right) \right. \\ \left. + R_u \left(\frac{s_{35}(t'_{14} + t'_{24}) - t_{13}t'_{14}}{s_{12}} + \frac{t'_{14}(s_{35} + t_{23}) - s_{35}s'_{45}}{t_{25}} \right. \right. \\ \left. \left. + \frac{t_{15}[s_{35}(2t'_{14} + t'_{24}) + t'_{14}t_{23}]}{s_{12}t_{25}} \right) \right], \quad (44)$$

where $s'_{ij} = s_{ij} - m_t^2$, $t'_{ij} = t_{ij} - m_t^2$, and all other terms may be obtained by crossing. Final-state QCD corrections are limited to the second term of $\Psi_{q\bar{q}}$, and thus this term does not appear in corrections to the leptonic final state. If the final state is massless, then the solution is recovered by setting $m_t = 0$, and noting that all primed invariants are equal to their unprimed counterparts.

A. Single-top-quark production via $W'_{R,L}$

In Sec. II A we saw that W' bosons tend to have a large branching fraction into top quarks. This observation leads us to consider the effect of such a W' on the size of the single-top-quark cross section at hadron colliders. In particular, we show the cross sections are large enough to improve the mass limits on W' bosons using data from run I of the Fermilab Tevatron. The W' boson affects the single-top-quark cross section through the three channels shown in Fig. 2. We concentrate on the s -channel production, because of the enhancement from the W' resonance. We do not present numerical results for the t -channel or associated production of a W' boson, because the cross sections for these channels are negligible for the masses we consider.

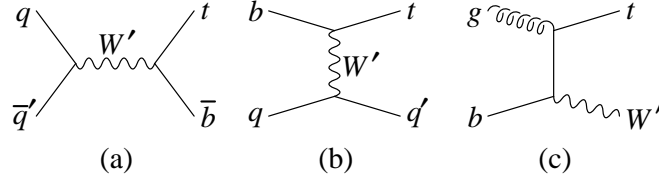


FIG. 2. Representative Feynman diagrams for single-top-quark production involving a W' boson: (a) s -channel production, (b) t -channel production, and (c) W' - t associated production.

In order to make definitive predictions, we stick to the assumption that the W' has purely right- or left-handed interactions. We choose the standard model CKM matrix as in Eq. (24), with the understanding that the final results may be scaled using the factorization of couplings in the last section. As in Sec. II A, we choose $m_t = 175 \pm 5$ GeV, $G_F = 1.16639 \times 10^{-5}$ GeV $^{-2}$, and $m_W = 80.4$ GeV. For leading-order cross sections we use CTEQ5L [36] leading-order parton distribution functions (PDFs). We use a two-loop running of α_s , and CTEQ5M1 PDFs for NLO cross sections. We use the LO and NLO widths calculated in Sec. II A in the LO and NLO cross sections, respectively, so that all terms are calculated at the same order and with the same method. We set both factorization and renormalization scales equal to $m_{W'}$, since most of the cross section will be produced near resonance.

We present the leading- and next-to-leading order cross sections for single-top-quark production, via $W'_{R,L}$ bosons of various masses, at run I of the Tevatron (a $p\bar{p}$ collider with $\sqrt{S} = 1.8$ TeV) in Tables IV and V. In Table IV we perform the calculation under the assumption that ν_R is too heavy for the W' to decay to leptons, and thus use the widths of Table II. In Table V we assume all decays are allowed, and use the widths of Table III. The cross sections

for just top-quark or antitop-quark production are one-half of the listed results. The corresponding single-top-quark cross sections at a run II of the Tevatron (a $p\bar{p}$ collider with $\sqrt{S} = 1.96$ TeV) appear in Tables VI and VII.

In Tables IV–VII we show the uncertainties in the cross sections due to the variation of the scale between $m_{W'}/2$ and $2m_{W'}$, the variation of the top-quark mass over $m_t = 175 \pm 5$ GeV including the effects of the change in width listed in Tables II and III, and uncertainties from the parton distribution functions (using a new method described in Sec. III B). Additional uncertainties come from the use of a vanishing bottom-quark mass, which overestimates the cross section by +1.5% at 200 GeV, but only +0.4% by 225 GeV, and is a negligible effect at higher W' masses. Extrapolating from the results of Ref. [39], we estimate that Yukawa corrections cause a shift of less than -1% in the cross section. The uncertainty from Monte Carlo statistics is 0.03%. There is a $\pm 4\%$ uncertainty in the NLO correction term from $\alpha_s = 0.118 \pm 0.005$. All uncertainties listed above are added in quadrature, and are presented for easy reference in the last column of each section in Tables IV–VII as a percentage error. If we had used the narrow width approximation, and multiplied the NLO W' cross section times NLO branching fraction to $t\bar{b}$ instead of evaluating the full matrix element, there would be an additional $\pm 1\text{--}2\%$ systematic uncertainty.

TABLE IV. LO and NLO cross sections in (pb) for $p\bar{p} \rightarrow W'_{R,L} \rightarrow t\bar{b} + \bar{t}b$ at run I of the Tevatron, $\sqrt{S} = 1.8$ TeV, when the decay to leptons is not allowed. Scale, top-quark mass, and PDF uncertainties are also listed in (pb). The last column in each section lists the total theoretical uncertainty in (%), where all uncertainties in the text and in this Table are added in quadrature.

Mass (GeV)	σ_{LO} (pb)	$\delta\sigma_{\text{LO}}(\mu, \delta m_t, \text{PDF})$ (pb)			$\delta\sigma_{\text{LO}}^{\text{Tot}}$ (%)	σ_{NLO} (pb)	$\delta\sigma_{\text{NLO}}(\mu, \delta m_t, \text{PDF})$ (pb)			$\delta\sigma_{\text{NLO}}^{\text{Tot}}$ (%)
200	32.24	+2.0 -1.8	+10.9 -9.8	+1.3 -1.2	+34.7 -31.2	50.90	+3.0 -2.4	+16 -15	+2.1 -1.9	+32.3 -30.2
225	51.45	+3.6 -3.2	+7.5 -7.4	+2.3 -2.0	+16.8 -16.2	77.24	+4.3 -3.6	+10 -10	+3.4 -3.0	+14.9 -14.4
250	52.29	+4.1 -3.6	+4.4 -4.5	+2.5 -2.1	+12.5 -11.8	76.10	+4.1 -3.6	+5.9 -6.1	+3.6 -3.0	+10.7 -10.2
275	45.58	+3.9 -3.4	+2.5 -2.6	+2.3 -1.9	+11.4 -10.3	64.92	+3.4 -3.1	+3.3 -3.4	+3.3 -2.7	+9.0 -8.4
300	37.18	+3.4 -2.9	+1.5 -1.6	+2.0 -1.6	+11.4 -9.9	52.11	+2.8 -2.6	+1.9 -2.0	+2.8 -2.2	+8.6 -7.7
350	22.82	+2.4 -2.0	+0.56 -0.58	+1.4 -1.1	+12.5 -10.4	31.20	+1.7 -1.6	+0.70 -0.73	+1.9 -1.4	+8.6 -7.4
400	13.46	+1.5 -1.3	+0.23 -0.23	+0.91 -0.68	+13.2 -11.1	18.04	+1.03 -0.98	+0.28 -0.29	+1.22 -0.91	+9.1 -7.7
450	7.836	+0.98 -0.82	+0.10 -0.10	+0.59 -0.44	+14.7 -12.0	10.31	+0.62 -0.59	+0.12 -0.12	+0.78 -0.58	+9.8 -8.2
500	4.537	+0.61 -0.51	+0.045 -0.046	+0.39 -0.28	+16.0 -12.9	5.873	+0.38 -0.36	+0.054 -0.056	+0.50 -0.37	+10.8 -9.0
550	2.617	+0.38 -0.31	+0.022 -0.022	+0.26 -0.18	+17.6 -13.8	3.335	+0.23 -0.21	+0.026 -0.027	+0.33 -0.23	+12.2 -9.5
600	1.503	+0.23 -0.19	+0.011 -0.011	+0.17 -0.12	+19.1 -15.0	1.889	+0.14 -0.13	+0.013 -0.013	+0.21 -0.15	+13.4 -10.6
650	0.859	+0.14 -0.11	+0.006 -0.006	+0.11 -0.07	+20.8 -15.2	1.066	+0.08 -0.08	+0.007 -0.007	+0.13 -0.09	+14.4 -11.4

TABLE V. LO and NLO cross sections in (pb) for $p\bar{p} \rightarrow W'_{R,L} \rightarrow t\bar{b} + \bar{t}b$ at run I of the Tevatron, $\sqrt{S} = 1.8$ TeV, when decays to quarks or leptons are both included. Scale, top-quark mass, and PDF uncertainties are also listed in (pb). The last column in each section lists the total theoretical uncertainty in (%), where all uncertainties in the text and in this Table are added in quadrature.

Mass (GeV)	σ_{LO} (pb)	$\delta\sigma_{\text{LO}}(\mu, \delta m_t, \text{PDF})$ (pb)				$\delta\sigma_{\text{LO}}^{\text{Tot}}$ (%)	σ_{NLO} (pb)	$\delta\sigma_{\text{NLO}}(\mu, \delta m_t, \text{PDF})$ (pb)				$\delta\sigma_{\text{NLO}}^{\text{Tot}}$ (%)
200	21.91	+1.4 -1.3	+7.3 -6.5	+0.91 -0.84	+34.2 -30.5		34.94	+2.0 -1.7	+11.1 -10.1	+1.5 -1.3	+32.7 -29.6	
225	35.05	+2.5 -2.2	+5.2 -5.1	+1.5 -1.4	+17.0 -16.4		53.36	+2.9 -2.5	+7.5 -7.4	+2.4 -2.1	+15.8 -15.3	
250	36.15	+2.8 -2.5	+3.2 -3.2	+1.7 -1.4	+12.7 -11.9		53.40	+2.9 -2.5	+4.4 -4.5	+2.5 -2.1	+11.1 -10.6	
275	31.92	+2.7 -2.4	+1.9 -1.9	+1.6 -1.3	+11.5 -10.5		46.14	+2.4 -2.2	+2.5 -2.6	+2.3 -1.9	+9.2 -8.6	
300	26.31	+2.4 -2.1	+1.2 -1.2	+1.4 -1.1	+11.5 -10.1		37.41	+2.0 -1.8	+1.5 -1.6	+2.0 -1.6	+8.7 -7.9	
350	16.40	+1.7 -1.4	+0.44 -0.46	+0.98 -0.75	+12.3 -10.1		22.72	+1.2 -1.2	+0.56 -0.58	+1.4 -1.0	+8.6 -7.5	
400	9.773	+1.12 -0.95	+0.18 -0.19	+0.66 -0.49	+13.5 -11.2		13.26	+0.75 -0.72	+0.23 -0.24	+0.89 -0.67	+9.1 -7.8	
450	5.735	+0.72 -0.60	+0.081 -0.083	+0.44 -0.32	+14.8 -12.0		7.641	+0.46 -0.44	+0.10 -0.10	+0.58 -0.43	+9.9 -8.3	
500	3.343	+0.45 -0.37	+0.038 -0.039	+0.29 -0.21	+16.1 -12.8		4.380	+0.28 -0.27	+0.046 -0.047	+0.38 -0.27	+10.9 -8.9	
550	1.941	+0.28 -0.23	+0.018 -0.019	+0.19 -0.14	+17.5 -13.9		2.503	+0.17 -0.16	+0.022 -0.023	+0.24 -0.17	+11.9 -9.5	
600	1.122	+0.17 -0.14	+0.009 -0.009	+0.12 -0.09	+18.6 -14.9		1.427	+0.10 -0.10	+0.011 -0.011	+0.16 -0.11	+13.3 -10.5	
650	0.646	+0.11 -0.08	+0.005 -0.005	+0.08 -0.06	+21.1 -15.5		0.812	+0.06 -0.06	+0.006 -0.006	+0.10 -0.07	+14.4 -11.5	

TABLE VI. LO and NLO cross sections in (pb) for $p\bar{p} \rightarrow W'_{R,L} \rightarrow t\bar{b} + \bar{t}b$ at run II of the Tevatron, $\sqrt{S} = 1.96$ TeV, when the decay to leptons is not allowed. Scale, top-quark mass, and PDF uncertainties are also listed in (pb). The last column in each section lists the total theoretical uncertainty in (%), where all uncertainties in the text and in this Table are added in quadrature.

Mass (GeV)	σ_{LO} (pb)	$\delta\sigma_{\text{LO}}(\mu, \delta m_t, \text{PDF})$ (pb)			$\delta\sigma_{\text{LO}}^{\text{Tot}}$ (%)	σ_{NLO} (pb)	$\delta\sigma_{\text{NLO}}(\mu, \delta m_t, \text{PDF})$ (pb)			$\delta\sigma_{\text{NLO}}^{\text{Tot}}$ (%)
200	36.39	+2.1 -1.9	+12.3 -11.0	+1.5 -1.4	+34.6 -31.0	57.39	+3.2 -2.6	+18.4 -16.8	+2.3 -2.2	+33.1 -30.2
225	58.56	+3.8 -3.4	+8.5 -8.4	+2.5 -2.2	+16.5 -15.9	87.86	+4.6 -3.9	+11.8 -11.9	+3.7 -3.4	+15.6 -15.3
250	60.13	+4.3 -3.8	+5.0 -5.1	+2.7 -2.3	+11.9 -11.2	87.52	+4.5 -3.9	+6.8 -6.9	+3.9 -3.4	+11.1 -10.7
275	53.00	+4.1 -3.6	+3.0 -3.0	+2.5 -2.1	+10.7 -9.7	75.57	+3.8 -3.4	+3.9 -4.0	+3.6 -3.0	+9.6 -9.0
300	43.78	+3.7 -3.2	+1.8 -1.8	+2.2 -1.8	+10.7 -9.3	61.46	+3.1 -2.8	+2.3 -2.4	+3.1 -2.5	+9.0 -8.3
350	27.63	+2.6 -2.3	+0.68 -0.70	+1.6 -1.2	+11.3 -9.7	37.90	+1.9 -1.8	+0.85 -0.88	+2.1 -1.7	+8.8 -8.1
400	16.81	+1.8 -1.5	+0.28 -0.29	+1.05 -0.80	+12.5 -10.3	22.65	+1.2 -1.1	+0.35 -0.36	+1.4 -1.1	+9.3 -8.2
450	10.13	+1.2 -1.0	+0.13 -0.13	+0.70 -0.52	+13.8 -11.2	13.43	+0.76 -0.72	+0.15 -0.16	+0.93 -0.70	+9.9 -8.6
500	6.092	+0.76 -0.64	+0.060 -0.061	+0.47 -0.35	+14.7 -12.0	7.953	+0.47 -0.45	+0.072 -0.074	+0.62 -0.45	+10.7 -9.0
550	3.661	+0.49 -0.41	+0.030 -0.030	+0.32 -0.23	+16.0 -12.9	4.710	+0.30 -0.28	+0.035 -0.036	+0.41 -0.30	+11.6 -9.7
600	2.197	+0.32 -0.26	+0.015 -0.016	+0.21 -0.15	+17.4 -13.7	2.790	+0.18 -0.18	+0.018 -0.019	+0.27 -0.19	+12.4 -10.3
650	1.316	+0.20 -0.16	+0.0081 -0.0082	+0.14 -0.10	+18.6 -14.4	1.650	+0.11 -0.11	+0.010 -0.010	+0.18 -0.13	+13.4 -11.1
700	0.7855	+0.13 -0.10	+0.0045 -0.0045	+0.096 -0.067	+20.6 -15.3	0.974	+0.071 -0.069	+0.0054 -0.0055	+0.12 -0.08	+14.9 -11.6
750	0.4671	+0.080 -0.063	+0.0026 -0.0026	+0.063 -0.044	+21.8 -16.5	0.573	+0.043 -0.043	+0.0032 -0.0031	+0.077 -0.054	+15.9 -12.7
800	0.2767	+0.049 -0.039	+0.0015 -0.0015	+0.041 -0.028	+23.1 -17.4	0.337	+0.027 -0.027	+0.0019 -0.0019	+0.050 -0.034	+17.4 -13.5
850	0.1634	+0.030 -0.024	+0.0010 -0.0010	+0.026 -0.018	+24.3 -18.4	0.198	+0.016 -0.016	+0.0012 -0.0012	+0.032 -0.022	+18.5 -14.4
900	0.0963	+0.018 -0.014	+0.0006 -0.0006	+0.017 -0.011	+25.7 -18.5	0.116	+0.010 -0.010	+0.0008 -0.0008	+0.020 -0.014	+19.7 -15.4
950	0.0569	+0.011 -0.009	+0.0004 -0.0004	+0.010 -0.007	+26.1 -20.1	0.0688	+0.0059 -0.0060	+0.0006 -0.0006	+0.0127 -0.0084	+20.8 -15.6
1000	0.0339	+0.006 -0.005	+0.0003 -0.0003	+0.0064 -0.0042	+25.9 -19.3	0.0413	+0.0036 -0.0036	+0.0004 -0.0004	+0.0079 -0.0051	+21.4 -15.7

TABLE VII. LO and NLO cross sections in (pb) for $p\bar{p} \rightarrow W'_{R,L} \rightarrow t\bar{b} + \bar{t}b$ at run II of the Tevatron, $\sqrt{S} = 1.96$ TeV, when decays to quarks or leptons are both included. Scale, top-quark mass, and PDF uncertainties are also listed in (pb). The last column in each section lists the total theoretical uncertainty in (%), where all uncertainties in the text and in this Table are added in quadrature.

Mass (GeV)	σ_{LO} (pb)	$\delta\sigma_{\text{LO}}(\mu, \delta m_t, \text{PDF})$ (pb)			$\delta\sigma_{\text{LO}}^{\text{Tot}}$ (%)	σ_{NLO} (pb)	$\delta\sigma_{\text{NLO}}(\mu, \delta m_t, \text{PDF})$ (pb)			$\delta\sigma_{\text{NLO}}^{\text{Tot}}$ (%)
200	24.75	+1.4 -1.3	+8.3 -7.3	+0.99 -0.94	+34.6 -31.0	39.43	+2.2 -1.8	+12.5 -11.3	+1.6 -1.5	+32.7 -29.6
225	39.92	+2.6 -2.3	+6.0 -5.8	+1.7 -1.5	+16.5 -15.9	60.74	+3.2 -2.7	+8.5 -8.4	+2.6 -2.3	+16.1 -15.6
250	41.58	+3.0 -2.6	+3.7 -3.7	+1.9 -1.6	+11.9 -11.2	61.43	+3.1 -2.7	+5.0 -5.1	+2.7 -2.4	+11.3 -11.0
275	37.13	+2.9 -2.5	+2.2 -2.3	+1.8 -1.5	+10.7 -9.7	53.73	+2.7 -2.4	+3.0 -3.0	+2.5 -2.1	+9.8 -9.1
300	30.99	+2.6 -2.3	+1.4 -1.4	+1.6 -1.3	+10.7 -9.3	44.14	+2.2 -2.0	+1.8 -1.8	+2.2 -1.8	+9.1 -8.4
350	19.85	+1.9 -1.6	+0.54 -0.55	+1.11 -0.87	+11.3 -9.7	27.61	+1.4 -1.3	+0.68 -0.70	+1.5 -1.2	+8.8 -8.0
400	12.20	+1.3 -1.1	+0.23 -0.23	+0.76 -0.58	+12.5 -10.3	16.65	+0.88 -0.84	+0.28 -0.29	+1.04 -0.79	+9.3 -8.2
450	7.411	+0.86 -0.73	+0.10 -0.11	+0.52 -0.38	+13.8 -11.2	9.941	+0.56 -0.53	+0.13 -0.13	+0.69 -0.51	+9.9 -8.6
500	4.484	+0.56 -0.47	+0.050 -0.051	+0.35 -0.26	+14.7 -12.0	5.922	+0.35 -0.33	+0.061 -0.062	+0.46 -0.34	+10.6 -9.1
550	2.709	+0.36 -0.30	+0.025 -0.026	+0.24 -0.17	+16.0 -12.9	3.526	+0.22 -0.21	+0.030 -0.031	+0.31 -0.22	+11.6 -9.6
600	1.635	+0.23 -0.19	+0.013 -0.013	+0.16 -0.11	+17.4 -13.7	2.100	+0.14 -0.13	+0.016 -0.016	+0.20 -0.15	+12.4 -10.3
650	0.9849	+0.15 -0.12	+0.0071 -0.0072	+0.108 -0.076	+18.6 -14.4	1.250	+0.086 -0.084	+0.0085 -0.0087	+0.14 -0.10	+13.8 -11.3
700	0.5919	+0.095 -0.076	+0.0040 -0.0040	+0.072 -0.050	+20.6 -15.3	0.7428	+0.054 -0.053	+0.0048 -0.0049	+0.090 -0.063	+14.7 -11.8
750	0.3547	+0.060 -0.047	+0.0023 -0.0023	+0.048 -0.033	+21.8 -16.5	0.4410	+0.033 -0.033	+0.0029 -0.0029	+0.059 -0.041	+15.9 -12.6
800	0.2122	+0.037 -0.029	+0.0014 -0.0014	+0.031 -0.022	+23.1 -17.4	0.2619	+0.020 -0.020	+0.0018 -0.0018	+0.039 -0.027	+17.2 -13.5
850	0.1268	+0.023 -0.018	+0.0009 -0.0009	+0.020 -0.014	+24.3 -18.4	0.1558	+0.013 -0.013	+0.0012 -0.0012	+0.025 -0.017	+18.6 -14.4
900	0.0759	+0.014 -0.011	+0.0006 -0.0006	+0.0132 -0.0089	+25.7 -18.5	0.0932	+0.0077 -0.0077	+0.0008 -0.0008	+0.016 -0.011	+19.5 -15.0
950	0.0457	+0.009 -0.007	+0.0004 -0.0004	+0.0084 -0.0056	+26.1 -20.1	0.0564	+0.0047 -0.0047	+0.0006 -0.0006	+0.0104 -0.0069	+20.7 -15.4
1000	0.0279	+0.005 -0.004	+0.0003 -0.0003	+0.0053 -0.0035	+25.9 -19.3	0.0348	+0.0029 -0.0029	+0.0004 -0.0004	+0.0066 -0.0043	+21.2 -15.5

In Tables IV–VII we use $m_{W'}/2$ and $2m_{W'}$ to estimate the uncertainty due to the choice of scale μ . While this is a reasonable estimate, we show in Fig. 3 the scale dependence of the LO and NLO cross section for a typical mass $m_{W'} = 500$ GeV at run I of the Tevatron over the range $\mu = m_{W'}/5$ – $5m_{W'}$. Even though the scale only enters the LO cross section through the PDFs, the NLO cross section is much less scale dependent than the LO cross section. It is apparent from this figure that only at unnaturally small scales do the LO and NLO cross sections agree. This is typical of single-top-quark production [37,39], and Drell-Yan-like processes in general, where initial-state corrections act like new production modes.

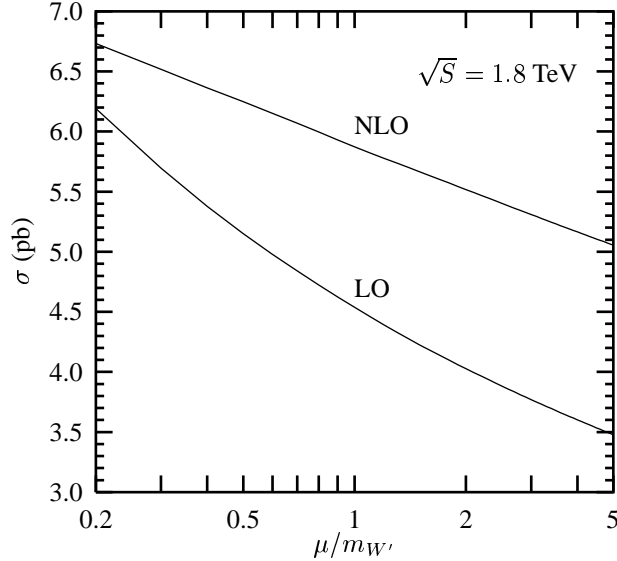


FIG. 3. Scale dependence of the leading-order (LO) and next-to-leading order (NLO) cross section $p\bar{p} \rightarrow W' \rightarrow t\bar{b}, \bar{t}b$ for $m_{W'} = 500$ GeV at run I of the Tevatron ($\sqrt{S} = 1.8$ TeV).

In Figs. 4 and 5, we show the LO and NLO single-top-quark cross sections, with $W'_{R,L}$ bosons, at the LHC as a function of $m_{W'}$. The cross sections are roughly a factor of 30 larger at the LHC than at the Tevatron due to the larger quark luminosity. For W' masses above 1 TeV, the cross section as a function of mass decreases slowly, leading to a much larger mass reach at the LHC. For example, the cross sections where quark and lepton decays are allowed are 580, 62, 9, and 2 fb, for 2, 3, 4, and 5 TeV W' bosons, respectively. Depending on detector performance, limits of 3–4 TeV on the W' mass should appear within a year or two of running at the initial luminosity of 10 fb^{-1} per year.

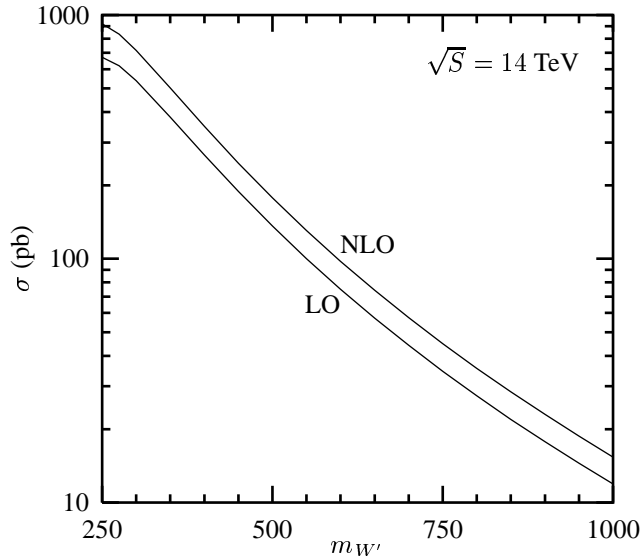


FIG. 4. Leading-order (LO) and next-to-leading order (NLO) cross section $pp \rightarrow W'_{R,L} \rightarrow t\bar{b}, \bar{t}b$ as a function of $m_{W'}$ at the LHC ($\sqrt{S} = 14$ TeV), when the decay to leptons is not allowed.

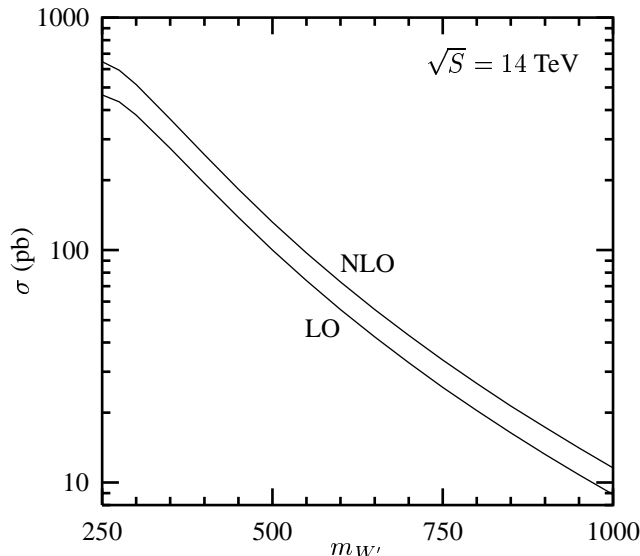


FIG. 5. Leading-order (LO) and next-to-leading order (NLO) cross section $pp \rightarrow W'_{R,L} \rightarrow t\bar{b}, \bar{t}b$ as a function of $m_{W'}$ at the LHC ($\sqrt{S} = 14$ TeV), when decays to quarks and leptons are both included.

B. Parton distribution function uncertainties

Because we are interested in heavy particles, the parton distribution functions (PDFs) will be probed at large values of the proton's momentum fraction. Hence, as opposed to Drell-Yan or s -channel single-top-quark production where the PDFs are well understood, we expect the PDF uncertainty to play a significant role in the total uncertainty of the cross section. In order to estimate the effects of this uncertainty we use a modification [40,41] of the “tolerance method” implemented in the CTEQ6 PDFs [42].

The tolerance method is based on diagonalization of the matrix of second derivatives for χ^2 (a Hessian matrix) near the minimum of χ^2 for the PDF fits [43]. Since χ^2 is approximately parabolic near its minimum χ_0^2 , hypersurfaces of constant χ^2 are hyperellipses in the space of the original 20 PDF parameters $\{a_i\}$. These hyperellipses are transformed into hyperspheres by a change of coordinates $\{a_i\} \rightarrow \{z_i\}$, $i = 1, \dots, 20$. The tolerance method assumes that all acceptable PDF sets correspond to a χ^2 that does not exceed their minimal value χ_0^2 more than by T^2 . As a result, the acceptable PDF sets have $\{z_i\}$ within a sphere of the radius T^2 around $\{z_i(\chi_0^2)\} \equiv \{z_i^0\}$. In principle, T should be chosen to correspond to a 1σ deviation of the fit. However, for simplicity we present results for $T = 10$, as used by the CTEQ6M101 – CTEQ6M140 PDF tables given in Ref. [42].

The PDF uncertainty for an observable O is the maximal change in O as a function of variables $\{z_i\}$ varying within the tolerance hypersphere. The CTEQ6 paper estimates the variation of O by using a master formula

$$\delta O = \frac{1}{2} \sqrt{\sum_{i=1}^{20} \delta O_i^2}, \quad \text{where } \delta O_i \equiv T \frac{\partial O}{\partial z_i} \approx T \frac{O(z_i^0 + t) - O(z_i^0 - t)}{t}, \quad (45)$$

and $t = 10$ is a step in the space of z_i . Here, $O(z_1^0, \dots, z_i^0 \pm t, \dots, z_{20}^0)$ is denoted as $O(z_i^0 \pm t)$. Eq. (45) is a good approximation for the PDF fits, but is less useful for observables, e.g. cross sections.

The difficulty with Eq. (45) is well exemplified for the problem at hand by Fig. 6. Here we see the uncertainty for each of the 20 pairs of PDFs as a function of the parameters z_i for $m_{W'} = 500$ GeV. If we apply Eq. (45) we would predict an uncertainty of $\pm 5.9\%$. However, $O(z_i^0 + t) - O(z_i^0 - t) \approx 0$ for nearly half of the parameters, even though Fig. 6 shows that these provide a large deviation. The uncertainty in Eq. (45) appears to be more sensitive to z_i which have a small absolute effect, but happen to cause a shift in the prediction which changes sign, than to large fluctuations. This defect of the master formula is a result of the simple observation that the PDF set that minimizes the uncertainty in a given observable O is not necessarily the same as the one that minimizes the fit to the global data set.

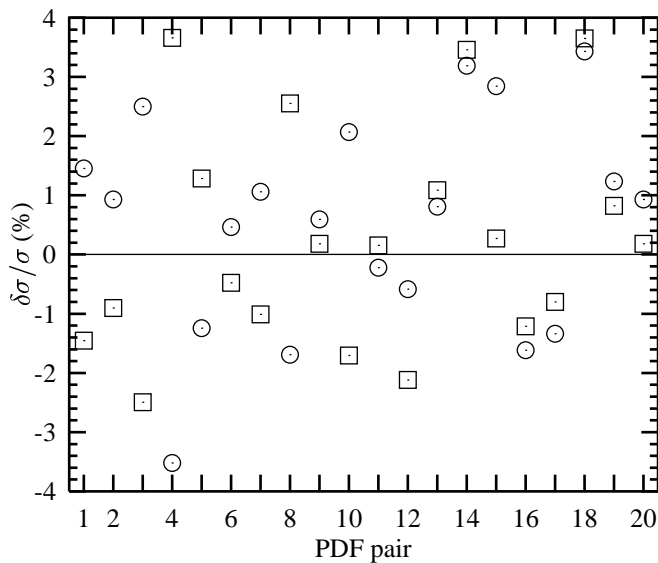


FIG. 6. Uncertainty in the cross section for $m_{W'} = 500$ GeV for each pair of PDFs using CTEQ6M1xx. Circles are odd PDF sets. Squares are even PDF sets.

In order to obtain a better estimator of the uncertainty of a generic observable O , we introduce [40,41] the “modified tolerance method” (MTM) master formula. We define the maximum positive and negative errors on an observable O by

$$\delta O_+ = \frac{T}{t} \sqrt{\sum_{i=1}^{20} \left(\max[O(z_i^0 + t) - O(z_i^0), O(z_i^0 - t) - O(z_i^0), 0] \right)^2}, \quad (46)$$

$$\delta O_- = \frac{T}{t} \sqrt{\sum_{i=1}^{20} \left(\max[O(z_i^0) - O(z_i^0 + t), O(z_i^0) - O(z_i^0 - t), 0] \right)^2}, \quad (47)$$

where the “tolerance” T is the same scaling parameter that determines the overall range of allowed variation of χ^2 , and we use $T = t = 10$ as in the CTEQ6 PDF sets. In Eqs. (46, 47) we sum the maximum deviations on the observable in each of the parameter directions, and hence retain both maximal sensitivity to the parameters that vary the most and estimate the range of allowed values of the cross section. Given the case in Fig. 6, we determine that $m_{W'} = 500$ GeV has an uncertainty of +8.6–6.2% — half again as large on the high side as estimated by the CTEQ method.

C. NLO Differential spectra

In the course of an experimental analysis it is common practice to normalize the number of events generated in an event generator by a “K-factor”. This K-factor is generally taken to be the ratio of the NLO to LO inclusive cross section. It is then assumed that turning on successive gluon radiation, called showering, in an event generator reproduces the correct shapes for the NLO distributions. While this is a reasonable approximation for the soft radiation that accompanies the jets, it does not always reproduce the spectrum of additional well-separated hard jets [44,45], or their effect on the primary jets. Since experimental reconstruction efficiencies depend on jet energies, it is important to have the most accurate prediction possible.

There are two main benefits of looking at the fully differential cross section. The first is that this provides a check on the jet distributions that come from the event generators. The second is that we see immediately whether the kinematic regions where perturbation theory breaks down are relevant to the measurable range of the distributions. The shape of the transverse momentum is especially important in studies with b -tags, since the tagging efficiencies depend on this variable.

In Figs. 7 and 8 we show the transverse momentum (p_T) distributions for the top-quark and bottom-jet, respectively, for $p\bar{p} \rightarrow W'^+ \rightarrow t\bar{b}$, and $m_{W'} = 500$ GeV at run I of the Tevatron. For comparison we plot both the NLO distributions and the LO distributions times a NLO K-factor of 1.29. The b -jet is reconstructed using a k_T cluster algorithm [46] to provide an infrared-safe way of combining partons. We use a k_T cone size of $\Delta R = 1$, similar to a fixed cone size of 0.7.

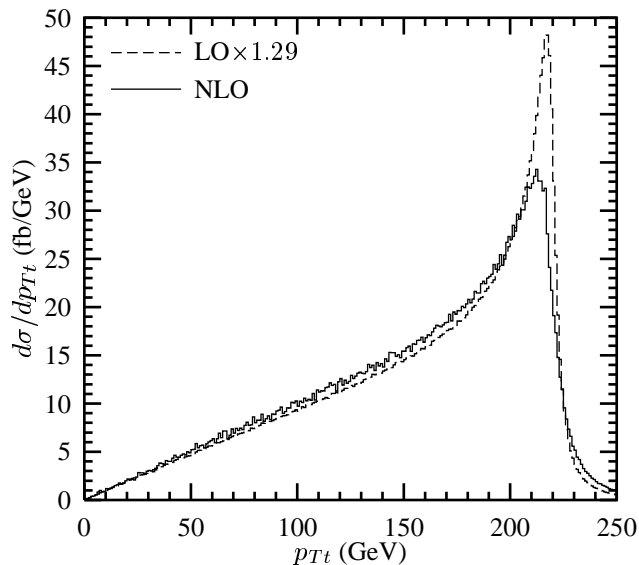


FIG. 7. Transverse momentum p_{Tt} distribution of the top-quark at NLO, and LO times a K-factor, for $m_{W'} = 500$ GeV.

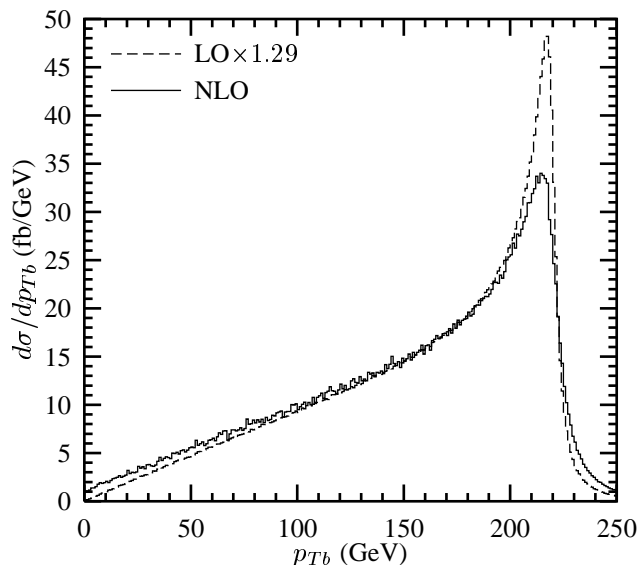


FIG. 8. Transverse momentum p_{Tb} distribution of the b -jet at NLO, and LO times a K-factor, for $m_{W'} = 500$ GeV.

As is generally the case, the p_T spectra of the b -jet and top-quark are somewhat softened at NLO. In the top-quark and b -jet p_T distributions in Figs. 7 and 8 there is a much improved behavior near the W' resonance at NLO. Aside from going to higher orders, it may be possible to further improve the shape in the resonance region by replacing the Breit-Wigner with a more dynamical form [47]. While there may be minor deviations at small transverse momentum due our choice of a massless bottom quark, the cross section vanishes at low p_{Tb} , and b -jet cannot be measured below about 10 GeV, so the effect will not be visible in the experiments. The pseudorapidity distributions of the top-quark and b -jet are shown in Figs. 9 and 10, respectively. The shapes of the distributions are so similar, that the LO curves are completely hidden by the NLO curves.

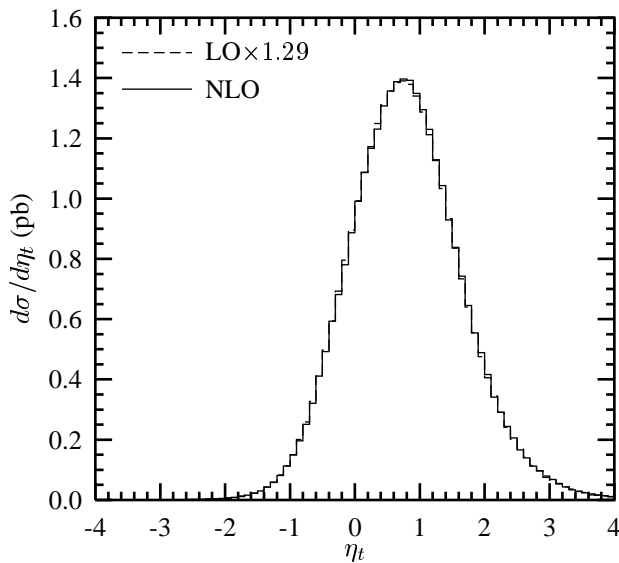


FIG. 9. Pseudorapidity η_t distribution of the top-quark at NLO, and LO times a K-factor, for $m_{W'} = 500$ GeV.

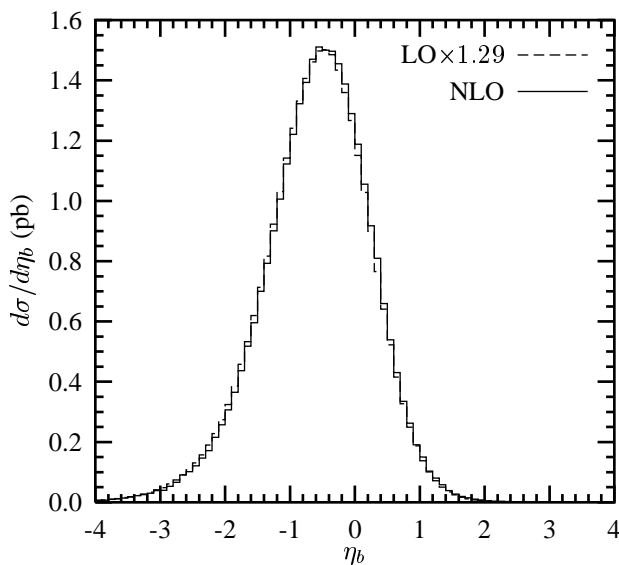


FIG. 10. Pseudorapidity η_b distribution of the b -jet at NLO, and LO times a K-factor, for $m_{W'} = 500$ GeV.

An important consideration is the effect of the choice of cone size on the shape of the transverse momentum distributions. In Fig. 11, we show the ratio of the p_T distributions of the b -jet for two common choices of $\Delta R = 0.54$ and 1.35 (which are similar to fixed cones of size 0.4 and 1.0, respectively) to our default choice of 1.0. When comparing distributions from event generators with NLO calculations, we must use the same jet definition. Otherwise, there can be a systematic shift in the shape of the distributions of 10–20%. This size of this effect is potentially larger than the effect of the jet-energy resolution on the reconstruction of jet shapes.

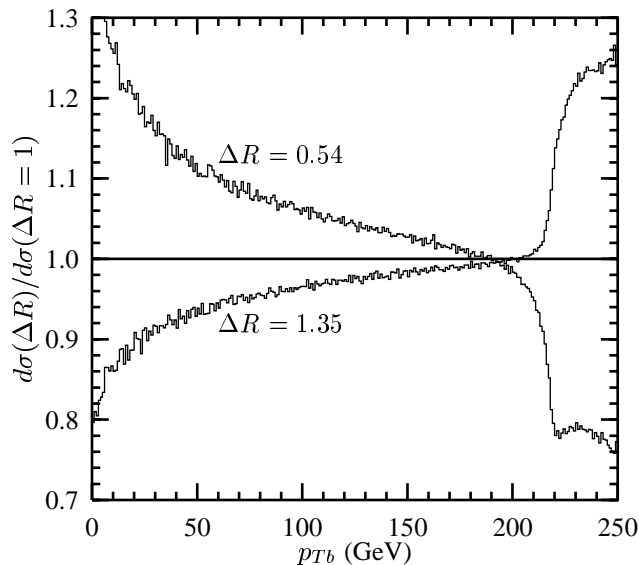


FIG. 11. Ratio of distributions of the transverse momentum of the b -jet using different k_T cone sizes at NLO.

The overall effect of the choice of cone size is only important for W' production right near resonance. The cross section is fairly small at lower transverse momentum, and thus changes in the shape in that region are not relevant. The effect at low p_T is further suppressed in an experiment, because b -tagging efficiency tends to be smaller at low p_T as well. In Fig. 12 we show the effect of different cone sizes on the p_{Tb} spectrum near the its peak at ~ 215 GeV, which corresponds to a 500 GeV W' resonance. Experimental analyses will concentrate on this resonant region. Hence, a mismatch of jet definitions could cause a systematic mistake in the comparison to the theoretical cross section of as much as $\pm 20\%$.

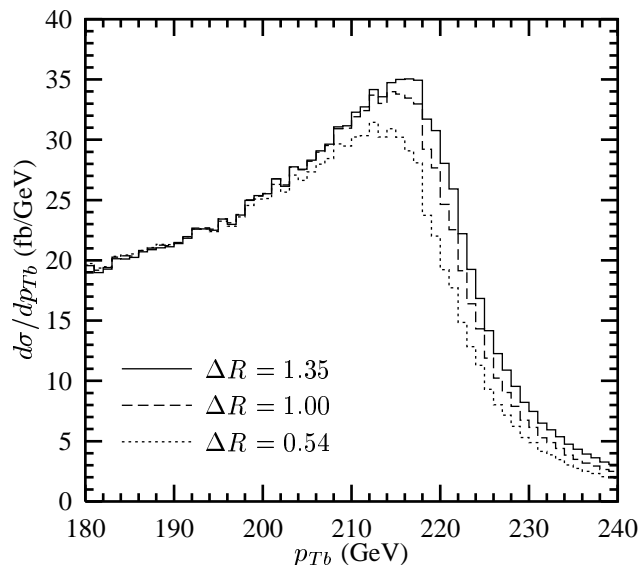


FIG. 12. Transverse momentum p_{Tb} distribution of the b -jet at NLO using three different cone sizes near the W' resonance region with $m_{W'} = 500$ GeV.

While the individual distributions for the W' boson are important, in an experimental analysis we want to fit for the mass of the W' boson. A likely strategy to find the W' is to look for a peak in invariant mass distribution $M_{t\bar{b}}$ of the top-quark/antibottom-jet pair. We do not perform a full analysis here, but simply show in Fig. 13 the $M_{t\bar{b}}$ distributions for $m_{W'} = 500$ GeV. The LO cross section is shown times the standard K-factor, but is divided by 2 to fit on the figure. While the central value of the peak has not shifted by much, there is a very large tail below the mass of the W' boson. Roughly half of the cross section is below the peak predicted at LO. Hard radiation at NLO has a much larger effect on the correlated distributions than we might naively expect from the 4% increase in the width. Almost $2/3$ of the LO distribution falls in a mass window of 500 ± 10 GeV, but only $1/2$ of the NLO distribution falls

in a mass window twice as wide, 500 ± 20 GeV. Hence, when considering the effectiveness of $M_{t\bar{b}}$, the reconstructible signal over background may be a factor of 2 smaller than predicted with a LO calculation.

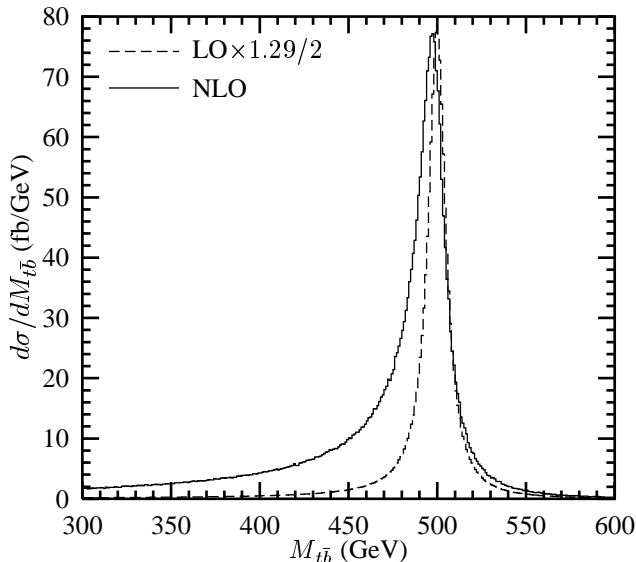


FIG. 13. Invariant mass distribution $M_{t\bar{b}}$ at NLO, and LO times a K-factor, for $m_{W'} = 500$ GeV.

The two distinguishing features of the W' cross section are that the b -jet and top-quark are each at a much larger transverse momentum than the dominant backgrounds, and there is a peak in the top-quark/antibottom-jet invariant mass distribution. While an optimized phenomenological analysis of the s -channel single-top-quark production cross section at the level of Ref. [48] is beyond the scope of this paper, we estimate the reach in W' mass using run I data in the following way: We begin with the recent limit on the s -channel single-top-quark cross section of ~ 17 pb [49,50]. Assuming that the W' boson adds directly to the standard model cross section, this immediately places a competitive bound of $m_{W'} \gtrsim 380$ –410 GeV (depending on the allowed decay modes). To improve this bound, we note that the invariant mass $M_{Wb\bar{b}}$ of the dominant $Wb\bar{b}$ background (B) scales like $1/M_{Wb\bar{b}}^4$. Hence, by reconstructing the W' invariant mass, and scaling the cross section limit by \sqrt{B} , we predict a 95% confidence-level limit of $m_{W'} \gtrsim 525$ –550 GeV should be attainable in a dedicated analysis of run I data. In run II of the Tevatron the s -channel single-top-quark cross section will be measured to $\pm 20\%$ with 2 fb^{-1} of integrated luminosity [48]. Given the very low backgrounds at large invariant masses, limits of 800–900 GeV may be reachable for W' bosons with standard-model size couplings.

IV. CONCLUSIONS

We present a fully differential calculation of W' boson production and decay at next-to-leading order in QCD. We demonstrate that the couplings of the W' to fermions factorize through NLO in the width, and in the complete two-to-two cross section. Any model that contains a new charged-current gauge particle, with arbitrary vector and axial-vector couplings, is described by the analytic results of Secs. II and III. In particular, the completely differential NLO cross section may be used to predict jet distributions for a given model in terms of $|V'_{f_i f_j}|$, R_t , and R_u . In most models, left-right mixing is either highly suppressed, or identically zero, which leads to a value of $R_u = 0$. Hence, by calculating R_t , we may translate the results for right- or left-handed W' bosons, appearing in Secs. III A and III C, into predictions for these models as well.

We use our calculation to estimate the effect of a left- or right-handed W' boson on the single-top-quark cross section. We show that the dominant uncertainties in the theoretical prediction come from the top-quark mass, higher-order QCD, and the parton distribution functions. In order to determine the PDF uncertainties, we propose the use of an improved modified tolerance method (MTM) that attains maximal sensitivity to the variance of the PDFs, and allows us to predict asymmetrical uncertainties. We present the NLO transverse momentum and pseudorapidity distributions of the top-quark and bottom-jet. We describe the effect of jet definitions on these distributions, and point out the strong sensitivity near the W' resonance region. We show that the correlated effect of additional hard radiation on the reconstruction of the W' mass peak can be much greater than naively expected from the increase in

the W' width.

We predict that the direct search limit on the mass of the W' boson may be improved by using data from runs I and II of the Fermilab Tevatron. By reconstructing the top-quark/bottom-jet invariant mass M_{tb} in the single-top-quark sample, a run I 95% confidence-level limit of $m_{W'} \gtrsim 525\text{--}550$ GeV should be attainable for standard-model-like couplings. At the end of run II, this limit may be pushed to 800–900 GeV. The signal at the LHC should be large enough to reach limits of at least 3–4 TeV. While these estimations are based on the known scaling of the backgrounds, a dedicated phenomenological analysis would be useful.

We conclude by applying our results to one specific example. In the top-flavor model of Ref. [6], the left-handed coupling in the W' - t - b vertex may be written as

$$g_L \sin \zeta V_{tb}^L = g \tan \phi V_{tb}. \quad (48)$$

The coupling to leptons, or the first and second generation of quarks, can be written

$$g_L \sin \zeta V_{f_i f_j}^L = g \cot \phi V_{f_i f_j}, \quad (49)$$

where g is the standard model $SU(2)_L$ coupling, and $V_{f_i f_j}$ is the CKM matrix or diagonal, for quarks or leptons, respectively. For masses of around 500 GeV, the angle ϕ is restricted to be small [51], $\sin^2 \phi < 0.05$. If we choose $\sin^2 \phi = 0.05$, the branching ratio into top quarks is 99%; virtually all of the decays of the W' will be into top quarks. The enhancement in branching fraction is exactly compensated by a decrease in production luminosity. The single-top-quark cross section has $R_t = \tan^2 \phi \cot^2 \phi R_t^{\text{SM}}$. Thus, the direct search limit for this top-flavor model will be identical to the one derived with standard-model couplings. If we wish to set a limit using a smaller value for $\sin^2 \phi$, the W' width will be the limiting factor in the mass reconstruction, and we should reevaluate the jet distributions in that scenario. By calculating $|V_{f_i f_j}^L|$, R_t , and R_u , and using our next-to-leading order results, we may now accurately compare any model containing a W' boson to direct experimental searches.

V. ACKNOWLEDGEMENTS

The author would like to thank S. Nandi and T. Tait for discussions regarding theoretical models, and P. Savard for experimental motivation. This work is supported by the U. S. Department of Energy under contract No. DE-AC02-76CH03000.

-
- [1] X. Li and E. Ma, Phys. Rev. Lett. **47**, 1788 (1981).
 - [2] E. Malkawi, T. Tait and C. P. Yuan, Phys. Lett. B **385**, 304 (1996).
 - [3] D. J. Muller and S. Nandi, Phys. Lett. B **383**, 345 (1996).
 - [4] H. Georgi, E. E. Jenkins and E. H. Simmons, Phys. Rev. Lett. **62**, 2789 (1989) [Erratum-ibid. **63**, 1540 (1989)].
 - [5] H. Georgi, E. E. Jenkins and E. H. Simmons, Nucl. Phys. B **331**, 541 (1990).
 - [6] H. J. He, T. Tait and C. P. Yuan, Phys. Rev. D **62**, 011702 (2000).
 - [7] A. Datta, P. J. O'Donnell, Z. H. Lin, X. Zhang and T. Huang, Phys. Lett. B **483**, 203 (2000).
 - [8] R. S. Chivukula, E. H. Simmons and J. Terning, Phys. Rev. D **53**, 5258 (1996).
 - [9] J. C. Pati and A. Salam, Phys. Rev. D **10**, 275 (1974).
 - [10] R. N. Mohapatra and J. C. Pati, Phys. Rev. D **11**, 566 (1975).
 - [11] R. N. Mohapatra and J. C. Pati, Phys. Rev. D **11**, 2558 (1975).
 - [12] G. Senjanovic and R. N. Mohapatra, Phys. Rev. D **12**, 1502 (1975).
 - [13] Y. Mimura and S. Nandi, Phys. Lett. B **538**, 406 (2002).
 - [14] M. Cvetcic and J. C. Pati, Phys. Lett. B **135**, 57 (1984).
 - [15] P. Langacker and S. Uma Sankar, Phys. Rev. D **40**, 1569 (1989).
 - [16] D. E. Groom *et al.* [Particle Data Group Collaboration], Eur. Phys. J. C **15**, 1 (2000).
 - [17] G. Arnison *et al.* [UA1 Collaboration], Phys. Lett. B **129**, 273 (1983).
 - [18] G. Arnison *et al.* [UA1 Collaboration], Europhys. Lett. **1**, 327 (1986).
 - [19] R. Ansari *et al.* [UA2 Collaboration], Phys. Lett. B **195**, 613 (1987).
 - [20] C. Albajar *et al.* [UA1 Collaboration], Z. Phys. C **44**, 15 (1989).
 - [21] F. Abe *et al.* [CDF Collaboration], Phys. Rev. Lett. **74**, 2900 (1995).

- [22] S. Abachi *et al.* [D0 Collaboration], Phys. Rev. Lett. **76**, 3271 (1996).
- [23] F. Abe *et al.* [CDF Collaboration], Phys. Rev. Lett. **84**, 5716 (2000).
- [24] T. Affolder *et al.* [CDF Collaboration], Phys. Rev. Lett. **87**, 231803 (2001).
- [25] J. Alitti *et al.* [UA2 Collaboration], Z. Phys. C **49**, 17 (1991).
- [26] J. Alitti *et al.* [UA2 Collaboration], Nucl. Phys. B **400**, 3 (1993).
- [27] F. Abe *et al.* [CDF Collaboration], Phys. Rev. D **55**, 5263 (1997).
- [28] E. H. Simmons, Phys. Rev. D **55**, 5494 (1997).
- [29] T. Tait and C. P. Yuan, arXiv:hep-ph/9710372.
- [30] R. Hamberg, W. L. van Neerven and T. Matsuura, Nucl. Phys. B **359**, 343 (1991).
- [31] R. V. Harlander and W. B. Kilgore, Phys. Rev. Lett. **88**, 201801 (2002).
- [32] D. Albert, W. J. Marciano, D. Wyler and Z. Parsa, Nucl. Phys. B **166**, 460 (1980).
- [33] T. Alvarez, A. Leites and J. Terron, Nucl. Phys. B **301**, 1 (1988).
- [34] A. B. Lahanas and V. C. Spanos, Phys. Lett. B **391**, 351 (1997).
- [35] B. W. Harris and J. F. Owens, Phys. Rev. D **65**, 094032 (2002).
- [36] H. L. Lai *et al.* [CTEQ Collaboration], Eur. Phys. J. C **12**, 375 (2000).
- [37] B. W. Harris, E. Laenen, L. Phaf, Z. Sullivan and S. Weinzierl, arXiv:hep-ph/0207055.
- [38] B. W. Harris, E. Laenen, L. Phaf, Z. Sullivan and S. Weinzierl, Int. J. Mod. Phys. A **16S1A**, 379 (2001).
- [39] M. C. Smith and S. Willenbrock, Phys. Rev. D **54**, 6696 (1996).
- [40] Z. Sullivan and P. M. Nadolsky, in *Proc. of the APS/DPF/DPB Summer Study on the Future of Particle Physics (Snowmass 2001)*, ed. R. Davidson and C. Quigg, arXiv:hep-ph/0111358.
- [41] P. M. Nadolsky and Z. Sullivan, in *Proc. of the APS/DPF/DPB Summer Study on the Future of Particle Physics (Snowmass 2001)*, ed. R. Davidson and C. Quigg, arXiv:hep-ph/0110378.
- [42] J. Pumplin, D. R. Stump, J. Huston, H. L. Lai, P. Nadolsky and W. K. Tung, arXiv:hep-ph/0201195.
- [43] J. Pumplin *et al.*, Phys. Rev. D **65**, 014013 (2002).
- [44] G. Corcella *et al.*, JHEP **0101**, 010 (2001).
- [45] T. Sjostrand, L. Lonnblad and S. Mrenna, arXiv:hep-ph/0108264.
- [46] S. D. Ellis and D. E. Soper, Phys. Rev. D **48**, 3160 (1993).
- [47] M. H. Seymour, Phys. Lett. B **354**, 409 (1995).
- [48] T. Stelzer, Z. Sullivan and S. Willenbrock, Phys. Rev. D **58**, 094021 (1998).
- [49] V. M. Abazov *et al.* [D0 Collaboration], Phys. Lett. B **517**, 282 (2001).
- [50] D. Acosta *et al.* [CDF Collaboration], Phys. Rev. D **65**, 091102 (2002).
- [51] E. Malkawi and C. P. Yuan, Phys. Rev. D **61**, 015007 (2000).